A New Observational Strategy for Monitoring the Tropical Cyclone Outflow Layer and its Relationship to Intensity and Structure Change

James D. Doyle
Naval Research Laboratory
Monterey CA 93943-5502
Phone: (831) 656-4716 Fax: (831) 656-4769 email: doyle@nrlmry.navy.mil

Peter G. Black
SAIC, Inc., Contractor at Naval Research Laboratory
7 Grace Hopper Avenue
Monterey, CA 93943-5502
Phone: (831) 656-5149/ Fax: (831) 656-5025 email: peter.black.ctr@nrlmry.navy.mil

LONG-TERM GOALS

The long-term goal of this project is to improve our understanding of the role of the outflow layer in tropical cyclone intensity and structure change though dedicated field program design and execution, improved observation of outflow structure and state of the art instrument development. The outflow layer is hypothesized to play both an active and passive role in tropical cyclone intensification and structural changes, and is investigated extensively using two highly instrumented NASA Global Hawk Unmanned Aerial Vehicles (UAVs), co-located observations from NOAA WP-3D, NOAA G-IV and Air Force WC-130J manned aircraft together with microwave, infrared and visible satellite imagers, radiometers and scatterometers from the Hurricane and Severe Storms Sentinel (HS3) field program in the Atlantic during 2012-2014

OBJECTIVES

The objectives of this research are as follows:

1. Observe the tropical cyclone secondary circulation including the outflow layer and inflow layer flows simultaneously utilizing emerging dropsonde technology.
2. Assist in the development and testing of a new generation of mini-dropsonde capable of sampling dozens of atmospheric profiles simultaneously from extreme altitudes of over 12 km and ranges in excess of 200 km with noise-free precision, accuracy exceeding present observational technology and better than 95% success rate (reliability).
3. Determine distribution of maximum cloud top heights from CloudSat radar and lidar observations and develop relationship with corresponding geostationary satellite observations of infrared-derived cloud top temperatures in the western north Atlantic and Pacific oceans in order to assist in development of requirements for tropical cyclone AUV over-flight capability.

Report Documentation Page

Form Approved
OMB No. 0704-0188

Public reporting burden for the collection of information is estimated to average 1 hour per response, including the time for reviewing instructions, searching existing data sources, gathering and maintaining the data needed, and completing and reviewing the collection of information. Send comments regarding this burden estimate or any other aspect of this collection of information, including suggestions for reducing this burden, to Washington Headquarters Services, Directorate for Information Operations and Reports, 1215 Jefferson Davis Highway, Suite 1204, Arlington VA 22202-4302. Respondents should be aware that notwithstanding any other provision of law, no person shall be subject to a penalty for failing to comply with a collection of information if it does not display a currently valid OMB control number.

1. REPORT DATE **30 SEP 2013**	2. REPORT TYPE	3. DATES COVERED **00-00-2013 to 00-00-2013**

4. TITLE AND SUBTITLE	5a. CONTRACT NUMBER
A New Observational Strategy for Monitoring the Tropical Cyclone Outflow Layer and its Relationship to Intensity and Structure Change	5b. GRANT NUMBER
	5c. PROGRAM ELEMENT NUMBER
6. AUTHOR(S)	5d. PROJECT NUMBER
	5e. TASK NUMBER
	5f. WORK UNIT NUMBER

7. PERFORMING ORGANIZATION NAME(S) AND ADDRESS(ES) **Naval Research Laboratory,7 Grace Hopper Avenue,Monterey,CA,93943-5502**	8. PERFORMING ORGANIZATION REPORT NUMBER

9. SPONSORING/MONITORING AGENCY NAME(S) AND ADDRESS(ES)	10. SPONSOR/MONITOR'S ACRONYM(S)
	11. SPONSOR/MONITOR'S REPORT NUMBER(S)

12. DISTRIBUTION/AVAILABILITY STATEMENT
Approved for public release; distribution unlimited

13. SUPPLEMENTARY NOTES

14. ABSTRACT

15. SUBJECT TERMS

16. SECURITY CLASSIFICATION OF:			17. LIMITATION OF ABSTRACT	18. NUMBER OF PAGES	19a. NAME OF RESPONSIBLE PERSON
a. REPORT **unclassified**	b. ABSTRACT **unclassified**	c. THIS PAGE **unclassified**	**Same as Report (SAR)**	**17**	

Standard Form 298 (Rev. 8-98)
Prescribed by ANSI Std Z39-18

APPROACH

Our approach is to design and execute a comprehensive field program that utilizes a new generation of high altitude observing platforms: the NASA Global Hawk AUV and high-altitude WB-57 manned aircraft- coupled with a new, cutting-edge mini-dropsonde observing technology for atmospheric vertical profiling from the stratosphere, across the upper-tropospheric outflow layer down to the lower-troposphere inflow layer.

WORK COMPLETED

1. *Observations of tropical cyclone outflow layer*
   Analysis of vertical structure of outflow layer jets for Hurricanes Leslie and Nadine in 2012 and Invest 97L in 2013 has been conducted using NCAR-EOL/Vaisala mini-dropsondes deployed from NASA AV-6 Global Hawk AUV. Observations were based on carefully planned Global hawk flight patterns in 2012 and 2013 the crossed evolving upper level outflow jets and their roots in inner-core supercell convection. Synthesis of outflow layer jet structure relative to inner-core supercell convection has been accomplished including relevance to hypothesized evolution of outflow channels during TC genesis and intensity change.

2. *Testing and evaluation of High Definition Sounding System (HDSS) and eXpendable Digital Dropsonde (XDD) system*
   Comparison of a new generation of dropsonde, the Yankee, Inc HDSS and XDD sonde was intercompared during CIRPAS Twin Otter test flights on 24-25 June, 2011 with NCAR-EOL/ Vaisala RD-94 conventional dropsonde and aircraft in-situ soundings. In addition surface sonde values were intercompared with NDBC data buoys offshore from Monterey and San Francisco. Follow-up sonde test deployments from a NASA DC-8 aircraft on 24 June offshore from Baja California and just to the east of TC Cosme in the eastern Pacific. These tests, while not intercompared with conventional sondes, showed a dramatic reduction in random noise and demonstrated the capability to receive profile data all the way to the surface from 42K ft as far as 200 km from the aircraft. An Additional XDD test deployments are planned for Oct, 2013 from the NASA WB-57 in the western Gulf of Mexico which are designed to be coincident with coastal radiosonde ascents.

3. *Distribution of, and relation between, tropical cyclone cloud top height and temperature*
   In order to address the feasibility of observations over tropical cyclones using Global Hawk aircraft, the distribution of cloud top heights observed from CloudSat W-band radar observations and associated geostationary satellite cloud top infrared temperatures from Naval Research Laboratory archives has been determine and a relation established that is accurate to within a standard deviation of 1K ft.

RESULTS

1. ***Observations of tropical cyclone outflow layer***
   A field program flight strategy was successfully conceived and executed that has provided observations of the vertical structure of the TC outflow layer and its attendant outflow jets. The complete TC secondary circulation illustrated in Fig. 1 was not resolved in 2012 due to RFI issues on the Global Hawk aircraft. These issues were resolved to a satisfactory degree in 2013 resulting in simultaneous observations of outflow layer and inflow layer structure. In 2012,

2

useable observations were confined to the TC outflow layer and focused on determination of structures along outflow jets as depicted in Fig. 2. Observations of jet structure during complete TC lifecycle await future observations. However, outflow jet structures in the near-steady state mature life cycle phase for Category 1 hurricanes Leslie and Nadine were obtained for the first time ever.
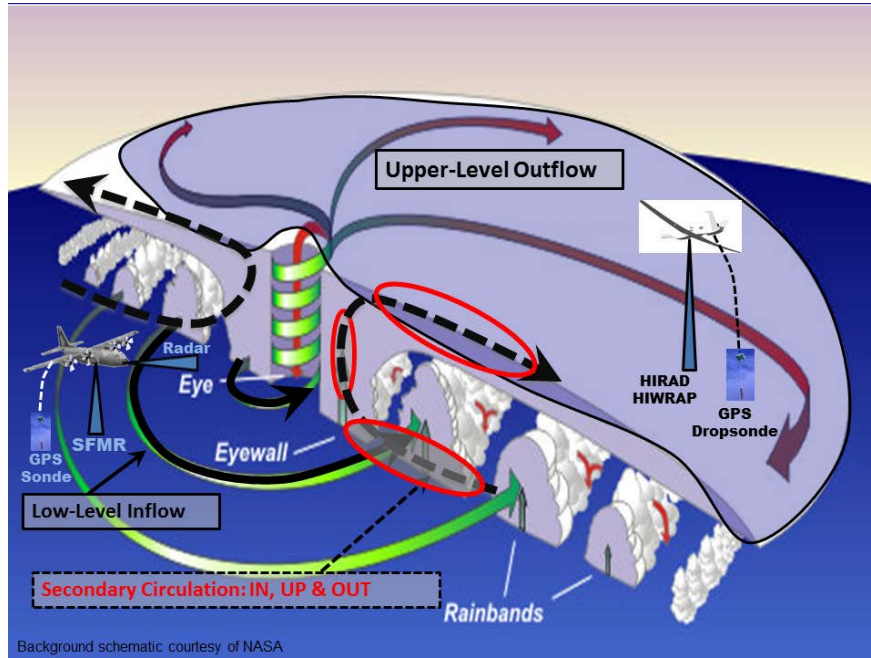

Figure 1. Schematic diagram of TC secondary circulation illustrating low-level inflow and upper-level outflow together with observing strategy of high-level Global Hawk UAV and low-level, inner-core WC-130J.
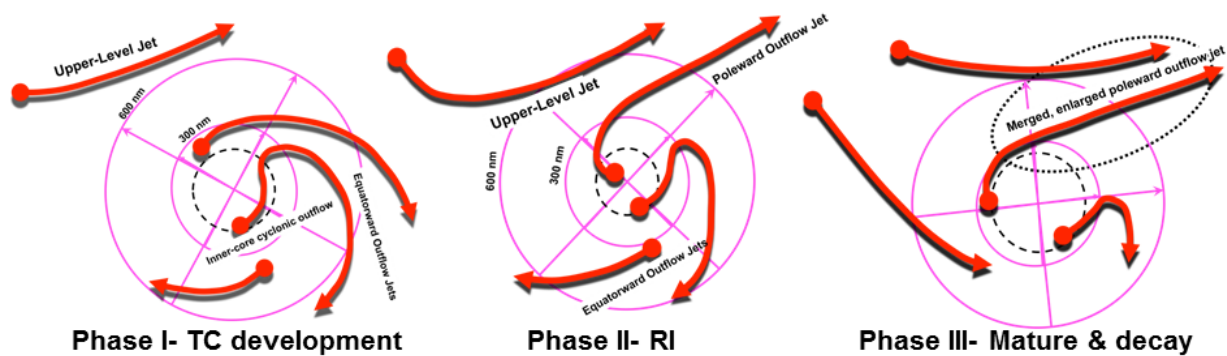
Figure 2. Hypothesized evolution of upper-level outflow jet structure from initial development Phase I with equatorial-directed jets, to Rapid Intensification (RI) Phase II with multiple equatorial- and poleward-directed jets to mature and decay Phase III with mainly poleward-directed jet.

The outflow structures in Leslie and Nadine were very different as illustrated in Fig. 3. Leslie, during her mature Cat 1 stage, was dominated by two diverging outflow jets similar to the Phase II schematic in Fig. 2. Nadine however, exhibited a single strong outflow jet emanating from an inner core super cell during her Phase II mature stage. This structure was also observed from sonde observations during the genesis Phase I stage of Invest 97L in 2013 prior to slow development of Hurricane Gabrielle.
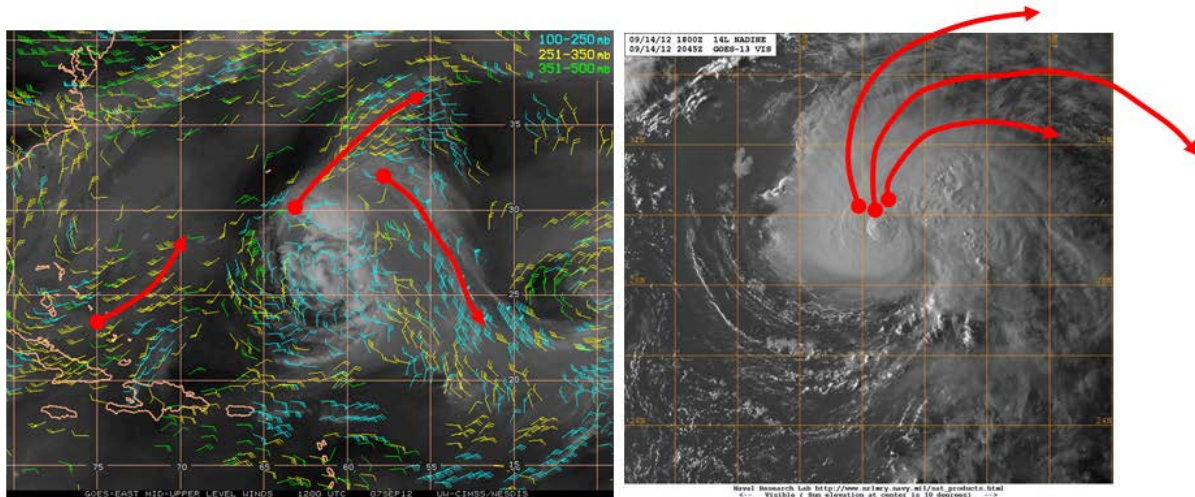

Figure 3. Hurricane Leslie outflow (left) on 7 Sept, 2012 showing divergent outflow jets resulting from environmental interaction: an example of possible ACTIVE outflow forcing broad region of inner-core convection. Hurricane Nadine on 14 Sept, 2012 (right) showing equatorial-directed outflow jet emanating from inner-core super-cell convection: an example of possible PASSIVE outflow being forced by convection.

The outflow structure for Leslie (Fig. 4) exhibited a prominent wind maximum just below the tropopause at the top of the cirrus cloud layer observed by the NASA Cloud Physics Lidar (CPL) with detailed fine structure as illustrated in Fig. 5. The strong shear above the wind max together with strong stability results in Richardson numbers at and below the critical value of ¼. This observation is repeatable over all 6 sondes deployed along the axis of the Leslie equatorward outflow jet. From this we conclude that Kelvin-Helmholtz instability must exist in this region, acting as a powerful mixing mechanism in the exchange of upper tropospheric and stratospheric air parcels.

In addition, these profiles also exhibit multiple, rather thin (500 m) constant wind layers below the wind max and within the cirrus cloud layer. Based on the fine structure detail of the cloud elements imaged by the CPL in Fig 5, we tentatively conclude that evaporative cooling at the base of the cirrus cloud layer may lead to these structures suggesting a second mechanism for mixing across the base of the outflow layer. Impacts of these mixing phenomena remain to be tested in future model experiments.
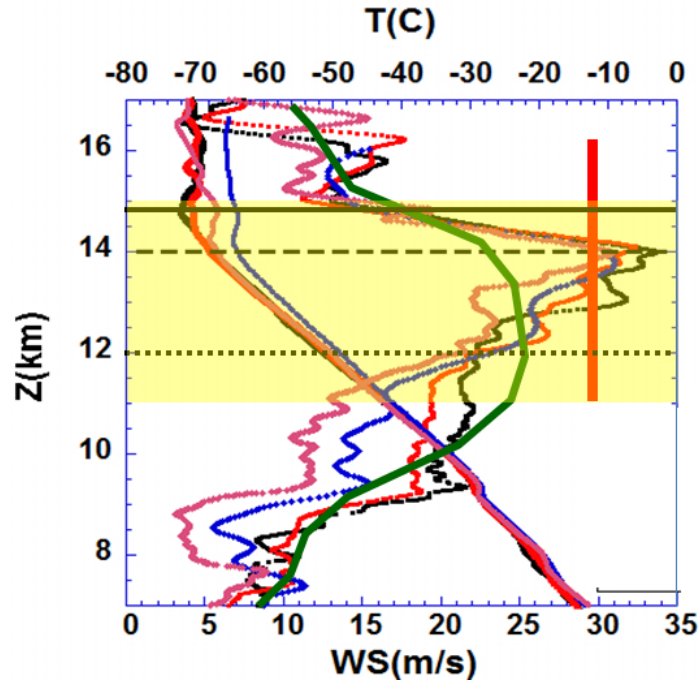
Figure 4. Upper-level wind speed and air temperature from four sequential dropsondes deployed along Hurricane Leslies equatorial-directed outflow jet on 7 Sept, 2012 from 1041-1111 UTC. Green line is COAMPS-TC model wind speed profile; Red line is satellite Atmospheric Motion Vector (AMV) vertical average; solid black is tropopause; dashed is cirrus top / jet max; dotted black is cirrus cloud base and yellow shading is cirrus cloud layer from NASA Cloud Physics Lidar (CPL).
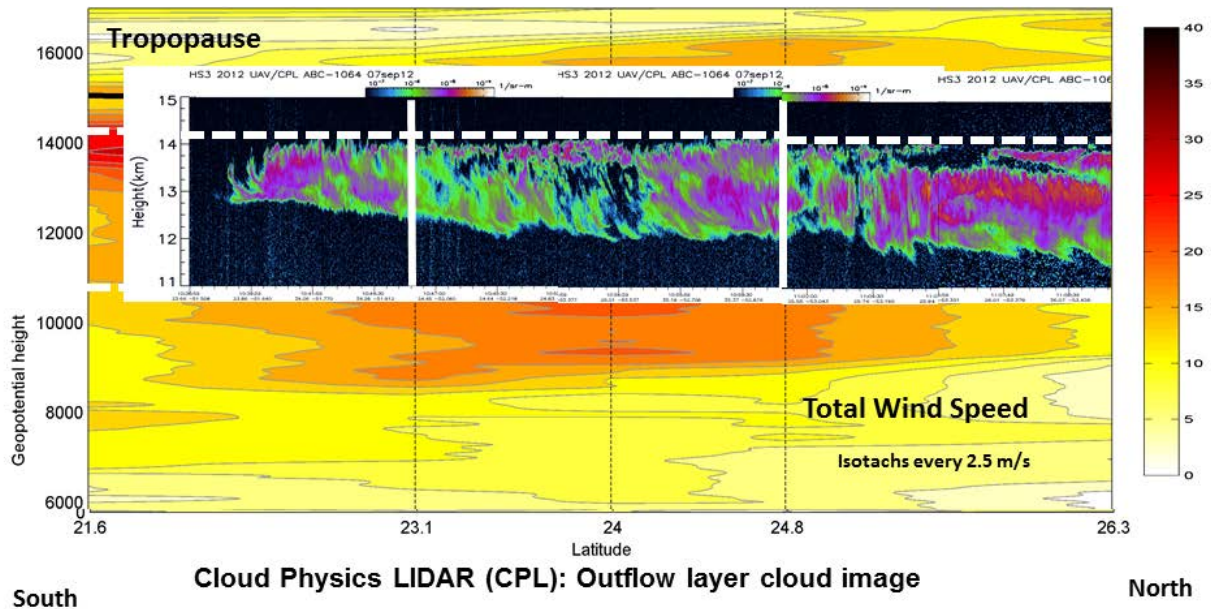

Figure 5. Cirrus cloud image from NASA Cloud Physics Lidar (CPL) backscatter supermposed upon along-jet wind speed analysis illustrating detailed fine structure features within outflow layer. Vertical dashed and solid white lines indicate dropsonde locations.

5

As mentioned above the outflow jet observed in Hurricane Nadine exhibited a very different morphology than the Leslie outflow jet. It emanate directly from an inner core supercell as illustrated in Fig. 6 with both dropsonds and upper level AMVs illustrating this feature. The dopsonde profiles through the outflow layer we however, very similar to those along the outflow jet in Leslie. In Nadine sonde profiles were available radially outward from the inner core within close proximity to the supercell. These profiles exhibited the same high shear above the outflow wind maximum and the multiple constant wind layers below the wind maximum. Since observations were available as a function of radius, these profiles illustrated details about the radial variation of the outflow layer. One may conclude from the six profiles indicated in Fig 6 and plotted in Fig 7 that the outflow layer thickness decreases radially outward as the outflow layer wind maximum increases, thus increasing the shear in the layer above the wind max and leading to super-critical Richardson numbers and K-H turbulence radially outward from the inner core. The Nadine profiles also show a significant secondary wind maximum just above the tropopause, the significance of which is unknown at present. Of note is that this structure is very similar to the primary and secondary wind maxima found in the air-sea boundary layer.
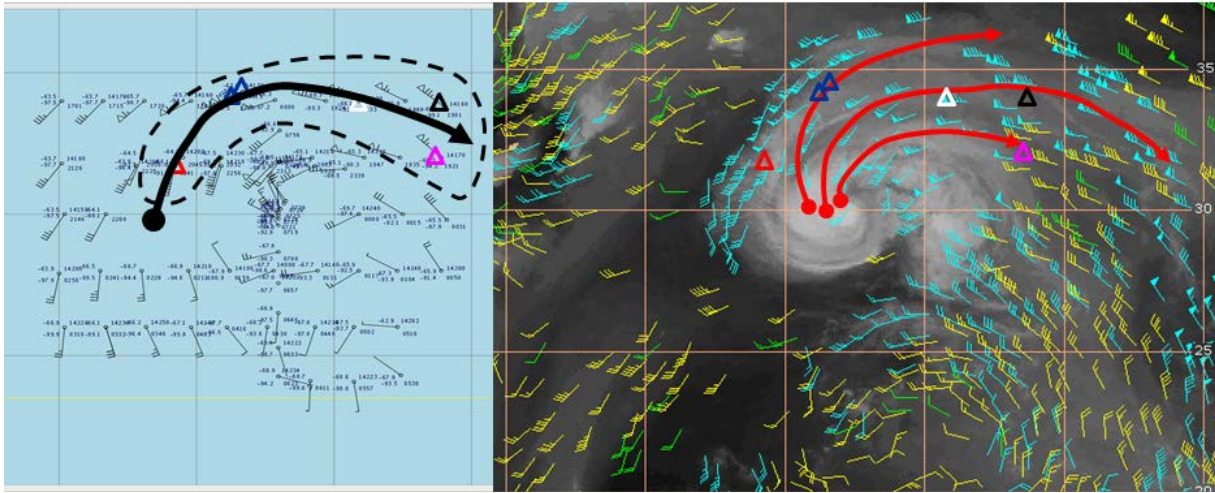

Figure 6. 150 mb outflow jet observed by AV-6 Global Hawk dropsondes (left) during flight over Hurricane Nadine on 14-15 Sept, 2012. The location of 6 dropsondes along the axis of the outflow jet are illustrated by colored triangles. Satellite-derived Atmopsheric Motion Vectors, (AMVs) illustrate outflow jet location (right) over mean layer from 11-16 km with jet-core sonde locations indicated by triangles.
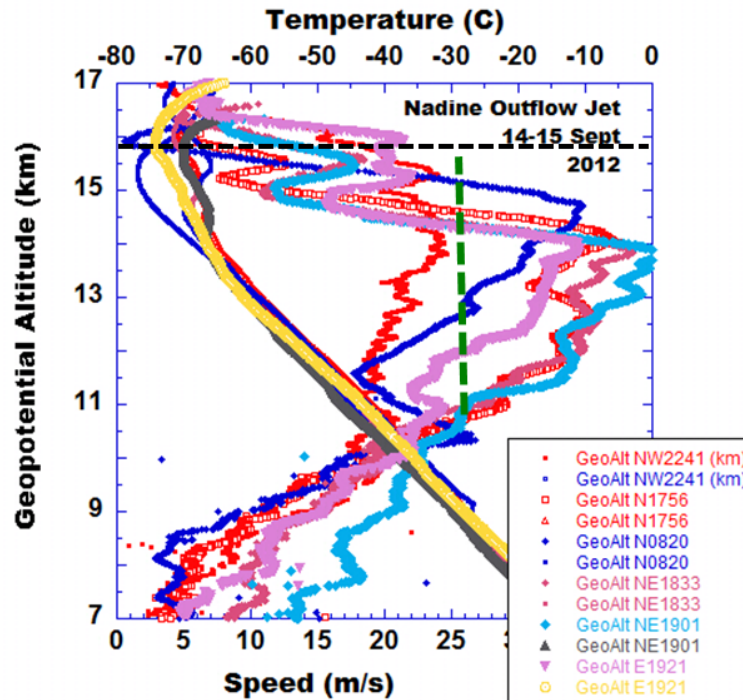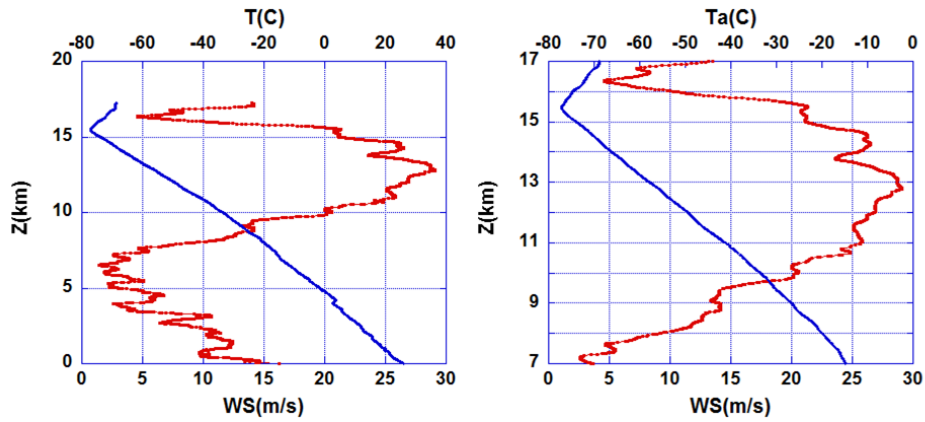
Figure 7. Temperature and wind speed profiles from 6 dropsondes along the outflow jet axis in Hurricane Nadine on 14-15 Sept, 2012. Dashed black line indicates tropopause just above double wind maximum in the outflow layer.

Although flights in 2013 were very limited, one flight into Invest 97L, the precursor to TD09 and Hurricane Gabrielle provided some addition profiles across the outflow jet of an incipient, slowly developing, pre-genesis disturbance. The structure of the outflow jet shown for 97L in Fig 8 illustrates the same type of structure as Nadine, i.e. a strong outflow jet emanating from an inner-core supercell. A schematic of this structure is illustrated in the lower right corner of Fig.8 and may be a precursor to the life cycle evolution hypothesized in Fig 2.
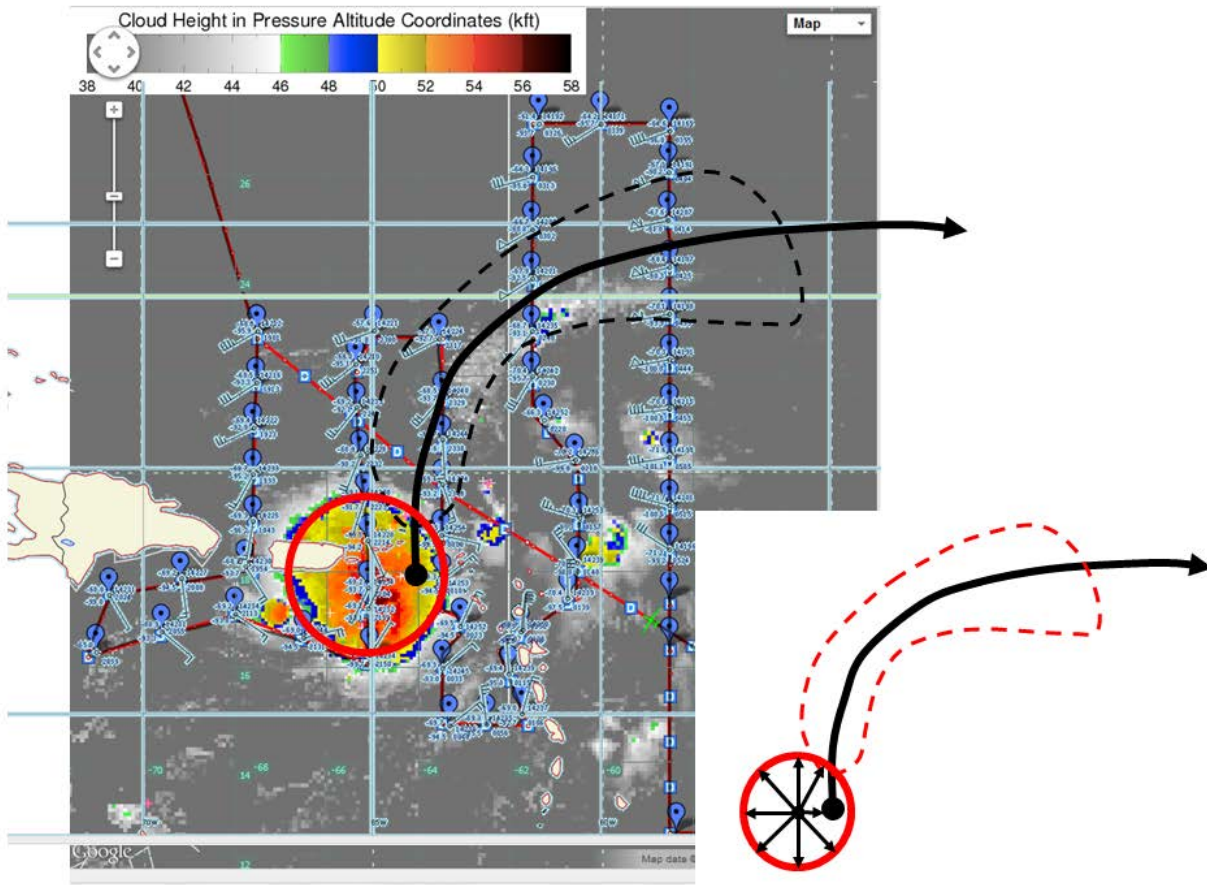
Figure 8. Dropsonde deployment across developing outflow jet over Invest 97L, precursor to TD10 and Hurricane Gabrielle on 4-5 Sept, 2013. Red circle indicates expanding supercell cloud shield, while dashed line indicates outflow jet winds in excess of 35 kt and solid black line indicates outflow jet axis. Schematic in lower right indicates composite outflow structure relative to supercell and outflow jet features comoposited from 97L (2013) and Nadine (2012).

In 2013 sonde antenna location was changed as well as the cabling for the dropsonde system which greatly reduced RFI effects to the point that most sondes functioned all the way to the surface, albeit with increase signal dropouts at low levels. However, as shown by Fig. 9 (left) both outflow structures and inflow structures are well resolved simultaneously, a large step forward in resolving the TC secondary circulation. At this stage of development, the outflow layer shown in more detail in Fig. 9 (right) is deeper with less fine structure than the Nadine and Leslie profiles.

Figure 9. Vertical temperature and wind speed profile along axis of outflow jet in 97L, 4-5 Sept, 2013 showing upper-level outflow jet together with low-level inflow jet just above the surface (left) and detailes of upper-level outflow jet with multiple thin layers possibly due to mixing events similar to those observed in Nadine and Leslie (2012).

2. ***Testing and evaluation of High Definition Sounding System (HDSS) and eXpendable Digital Dropsonde (XDD) system***

The first field test of a new generation of atmospheric profilers, the XDD dropsonde, was executed on June 24-25, 2011 in order to improve the capability of atmospheric profiling sondes in terms of low noise and multiple observations over short time periods. The new XDD sonde system has the capability for atmospheric profile measurements at least as accurate as the present widely used RD-94 unit and accompanying high resolution aircraft profiling as shown in Figs. 10-14. It is shown that the new XDD sonde is a low noise unit, suggesting it may set a new standard in profiling precision, with speed random noise on the order of one-half meter per second, wind direction noise on the order of 6 degrees, temperature noise on the order of one-quarter degree Celsius and relative humidity noise on the order of half a percent. The histograms and probability plots in Fig 14 show that the noise is log-normally distributed and a factor of two lower than differences amongst the sonde mean profiles. This is found to be superior to the current RD-94 dropsonde unit. Further improvements in the XDD were further demonstrated during a recent test of 7 XDD units deployed from a NASA DC-8 at altitude of 42K ft, which showed further reduction in random noise for all parameters and further illustrated the capability to transmit usable data from over 200 km away.
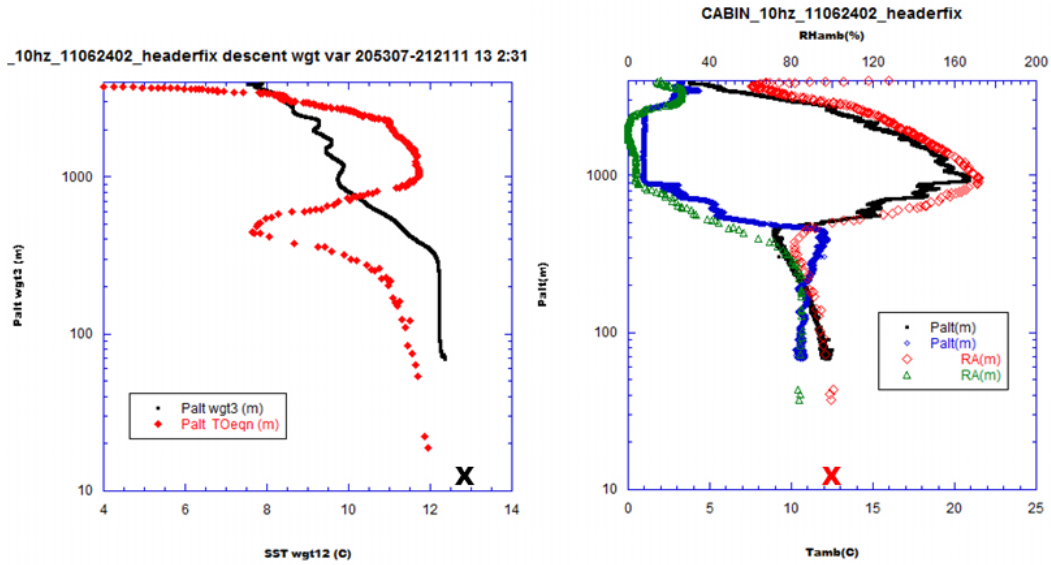
Figure 10. Comparison of smoothed XDD infrared SST profile with smoothed Twin Otter Infrared Radiation Thermometer (IRT) SST profile during spiral descent on 24 June over buoy 46042 (left panel). Air temperature and humidity (right panel) are shown in red and black for the XDD and TO air temperature, respectively and the humidities in green and blue. Buoy SST is indicated by the 'x' (left panel) and buoy air temperature by 'x' (right panel).
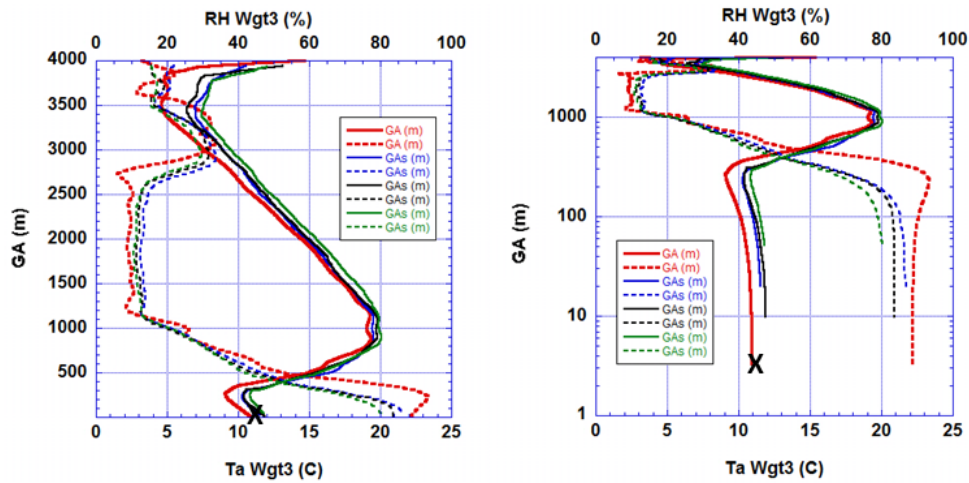

Figure 11. Comparison between YES XDD and Vaisala RD94 dropsonde observations from CIRPAS Twin Otter aircraft of Ta, air temperature (solid) and RH, relative humidity (dashed) during Flight 2, 25 June 2011vs linear geopotential height (left) and log geopotential height (right), designed to emphasize boundary layer detail. RD-94 data is in red, XDD data in blue, black and green. X is data from NDBC buoy 46042.
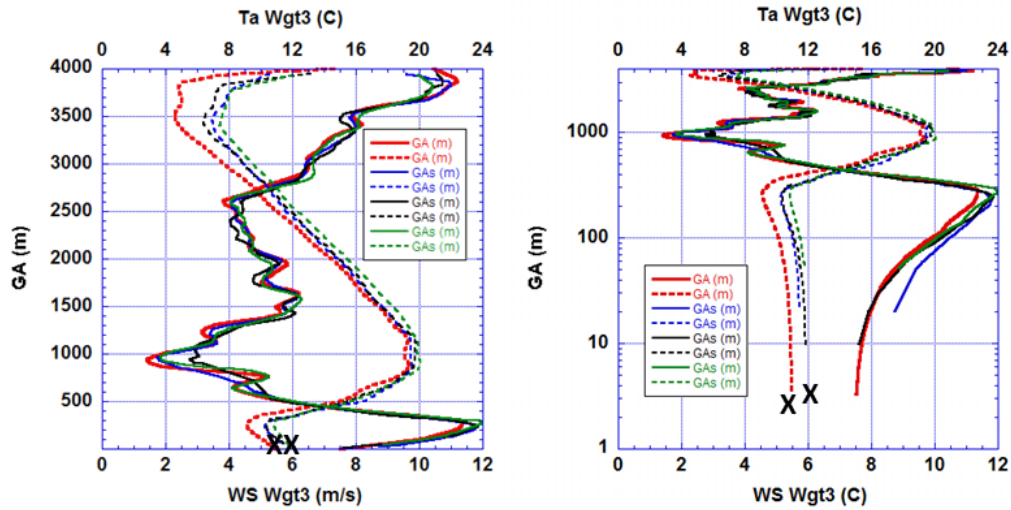
Figure 12. Comparison from CIRPAS Twin Otter aircraft between YES XDD and Vaisala RD94 dropsonde observations of wind speed (solid), WS and air temperature (dashed), Ta – Flight 2, 25 June 2011: linear geopotential height coordinates on the left, log coordinates, emphasizing boundary layer detail, on the right. Vaisala data is in red , YES data in Blue, black and green. X is data from NDBC buoy 46042.
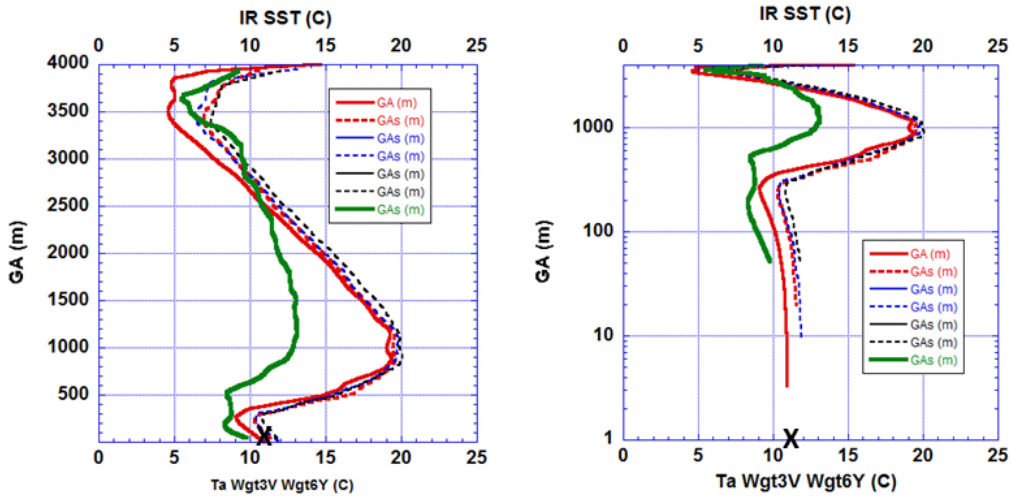
Figure 13. Comparison from CIRPAS Twin Otter aircraft between YES XDD and Vaisala RD94 dropsonde observations of air temperature, Ta, and XDD infrared-derived SST (solid green) from Flight 2, 25 June 2011: linear geopotential height coordinates on the left, log coordinates, emphasizing boundary layer detail, on the right. Vaisala Ta is in solid red , YES Ta is in dashed blue and black. X is SST from NDBC buoy 46042.
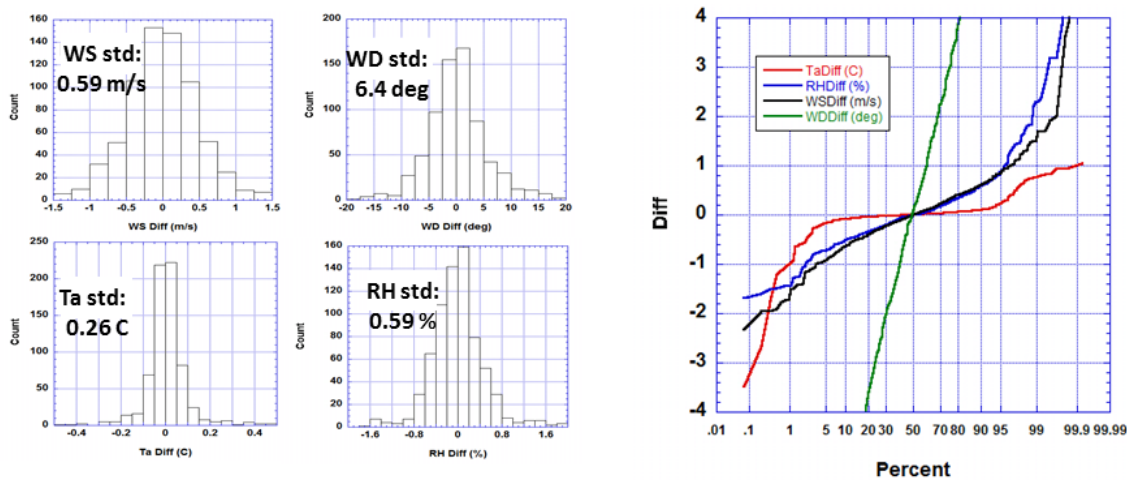
Figure 14. Histograms (left) of XDD noise distribution about 6-pt smoother average for a) wind speed (upper left), b) wind direction (upper right), c) air temperature (lower left) and relative humidity (lower right). XDD probability plot (right) of noise distributions for wind speed (black), wind direction (green) air temperature (red) and relative humidity (blue). The thick black line indicates the 95% confidence limits for the distributions.

Both the XDD and RD-94 sondes showed they were able to provide repeatable profile observations to within about the same accuracy as the white noise, with difference due mainly to real meteorological fluctuations in the variables. Comparison of the mean XDD profiles with the RD-94 and Twin Otter spiral descent observations showed that the XDD's were warmer by about 1C and drier by about 5% than the RD-94 and Twin Otter values. The twin Otter winds had to be heavily filtered due to oscillation associated with continuous heading changes during descent. However, the XDD and RD-94 winds were virtually identical during even small scale fluctuations in the vertical. The mean TO winds were also in good agreement although small scale fluctuations could not be resolved due to the required heavy filtering.

This experiment demonstrated promise for some new capabilities. In two of the XDD sondes, it was shown that the mini-radiometer had the capability for measuring skin SST to within 0.5C of in-situ moored buoy bulk SST at 1-m depth. Although by no means a conclusive sample, these initial results indicate promise for this new sensor. In addition, two other sondes were able to float on the surface for some tens of seconds and report air temperature observations that approached the mini-radiometer SST values. This two is a promising development in that proper design may allow for both radiometric SST values and in-situ values of SST to be observed.

Although the results of this intercomparison indicate a promising future for the XDD sonde design, it must be kept in mind that the conclusions above are based on a very small data sample: 10 XDD sondes, 14 RD-94 sondes and two aircraft spiral descents. It is anticipated that further testing can be accomplished in the near future to further substantiate our conclusions.

3.   Distribution of, and relation between, tropical cyclone cloud top height and temperature
In order to deploy dropsondes as discussed above, either XDD or RD94, assurances must be obtained that the aircraft can in fact fly safely over the tops of tropical cyclones. For safety reasons, NASA presently requires their GH aircraft to maintain minimum separation between cloud tops and aircraft of

5K ft. Given that AV-6 has a maximum altitude capability of 62K ft and AV-1 of 58K ft, the question must be asked whether or not a majority of TC's can in fact be successfully overflown by either GH aircraft.

In order to address this issue a data set of 9 years of CloudSat W-band radar derived observations of maximum cloud top height over tropical cyclones was examined in detail. This data set was matched with the TC infrared cloud top temperature image archive maintained at the Naval Research Laboratory. 62 western Pacific TC cases of Cloudsat overpasses over the TC eyewall or TC principal rainband were examined. Image intercomparisons similar to that shown in Fig. 15 were utilized to establish histograms of cloud top height and of cloud top temperature. Statistical probability plots derived from these histograms are shown in Fig. 16. These diagrams show that cloud top heights over rainbands tend to have a flatter distribution than those over TC eyewalls. The means are similar at about 51K ft. However the 95% confidence levels range from 54K ft over TC bands to 57K ft over TC eyewalls.

A simple quadratic relationship between cloud top temperature available hourly via geostationary infrared sensors and cloud top height from CloudSat was derived, i.e.Fig 17 (left), that shows a well-defined relationship. Fig 17 (right) shows that this relation is accurate to within a standard deviation of ±1K ft, or 95% confidence limit of ±3 K ft.
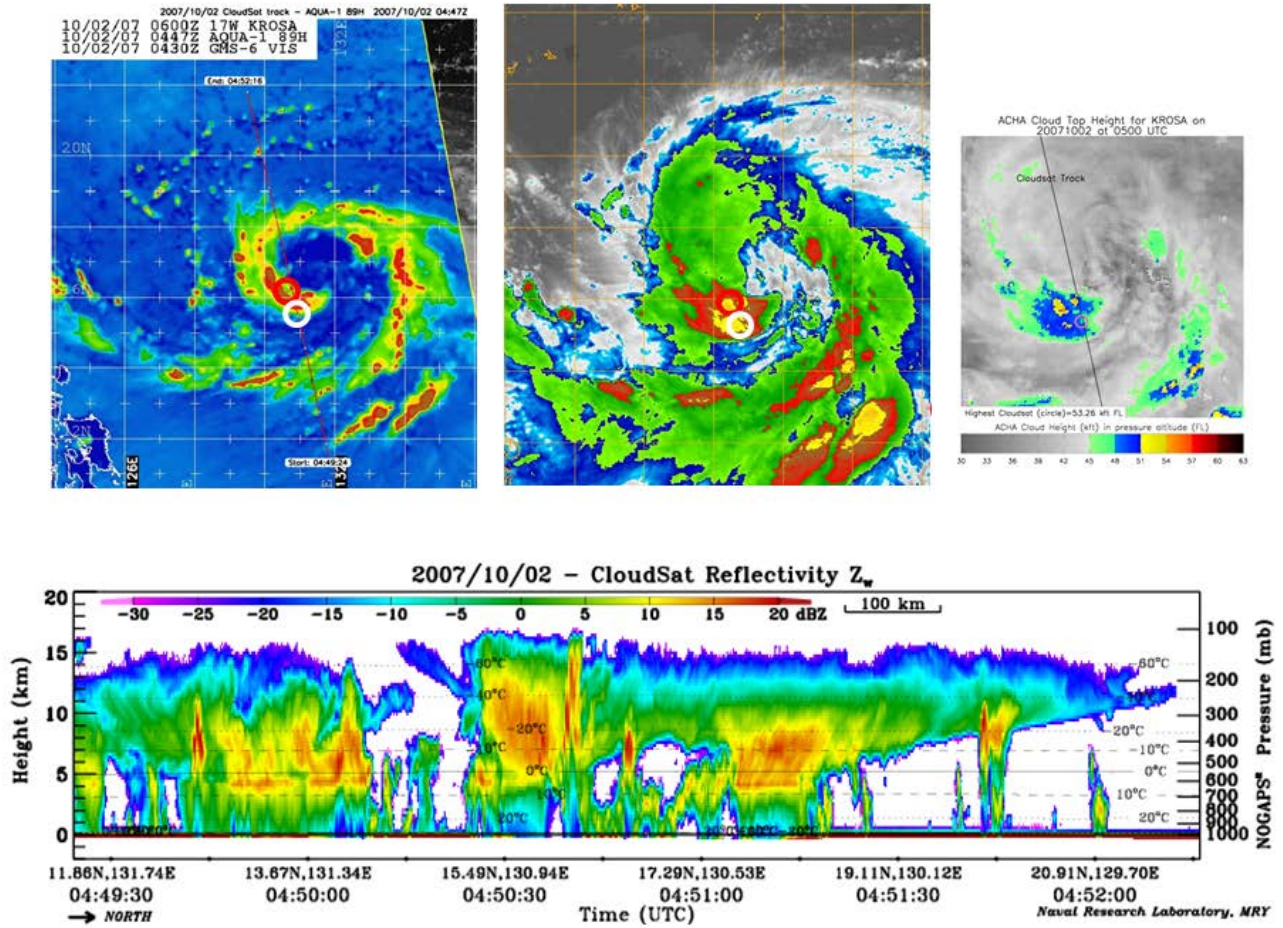
Figure 15. Example of CloudSat pass over Typhoon Krosa showing observations of W-band radar reflectivity (bottom), and satellite ground track superimposed on AQUA 89 GHz passive microwave image, used to estimate cloud top height for an 9-year data sample from 2002-20010. Center panel shows infrared cloud top temperature distribution while left panel shows cloud top heights derived from relation between cloud top height and IR temperature.
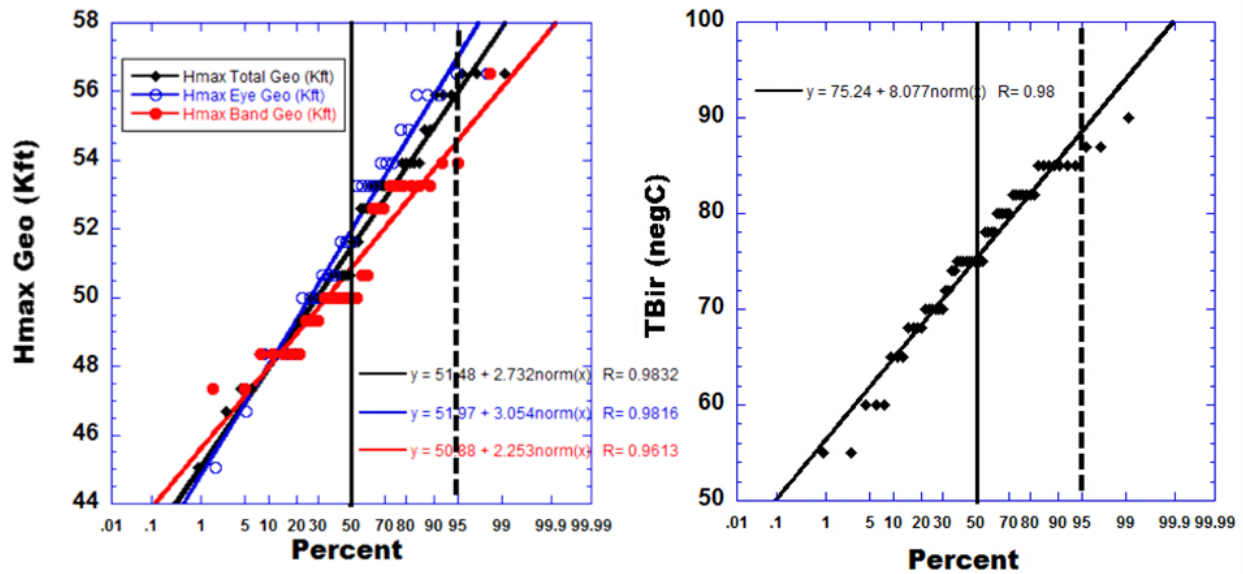
14

Figure 16. Probability plot (left) of 9 year sample of CloudSat W-band radar-derived cloud top heights for the TC eyewall (blue), principal band (red) and total (black) showing medial value of 51K ft and maximum of 57K ft. Corresponding probability plot for infrared cloud top temperature is shown in right panel. All distributions are approximately log-normal, indicated by linear fits.
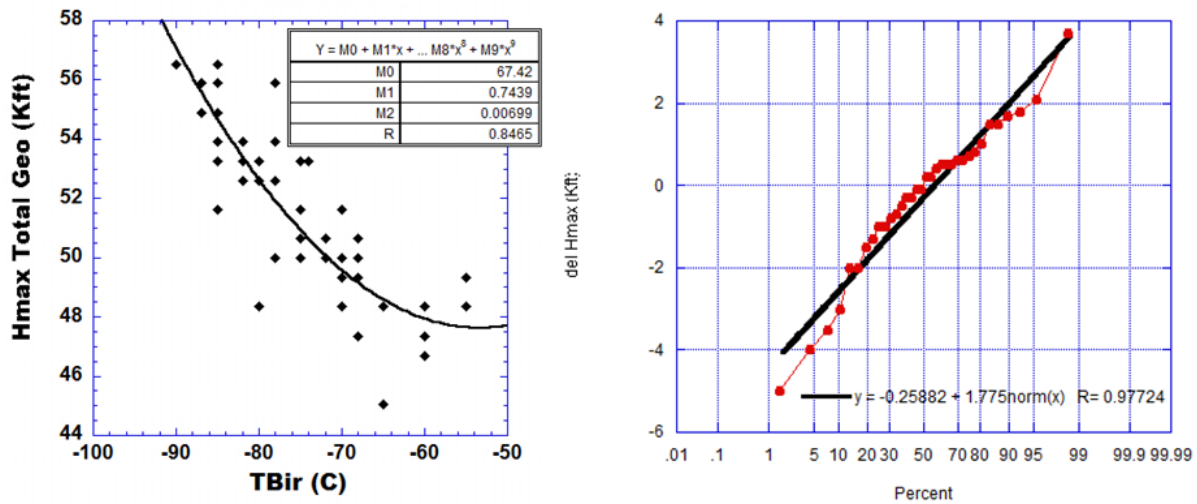

Figure 17. Quadratic relation between cloud top height and infrared cloud top temperature (left). Probability plot (right) of deviations about log-normal curve fit showing standard deviation of ±1K ft and 95% confidence level of ±3Kft.

RELATED PROJECTS

This project provides valuable observational input to COAMPS-TC project N0001412WX20683 entitled: Improvement of High-Resolution Tropical Cyclone Structure and Intensity Forecasts using COAMPS-TC and to satellite studies project 75-4838-0-3-5, entitled Defense Weather Satellite follow-on Analysis of Alternatives (AoA), sponsored by the U. S. Air Force.

PUBLICATIONS

Refereed Publications: Submitted or appeared.

1. Doyle, James, Yi Jin, Richard Hodur, Sue Chen, Hao Jin, Jon Moskaitis, Alex Reinecke, Peter Black, J. Cummings, E. Hendriks, T. Holt, C-S. Liou, M. Peng, C. Reynolds, K. Sashegyi, J. Schmidt and S. Wang2012: Real-Time Tropical Cyclone Prediction Using COAMPS-TC**, *AOGS Advances in Geosciences*, **28**, Eds. Chun-Chieh Wu and Jianping Gan, World Scientific Publishing Company, Singapore, 15-28.

2. Pun, Iam-Fei, I-I Lin, Peter G. Black and Dong-Shan Ko, 2012: Regression-Derived Satellite-Based Upper Ocean Thermal Structure for the Western North Pacific Typhoon Research, *Progress in Oceanography*, in review.

3. Black, P. G., 2012: Tropical Cyclone Unusual Intensity and Structure Change in the Western North Pacific Observed by Reconnaissance Aircraft During TPARC/TCS08 and ITOP/TCS10**, *J. Tropical Cyclone Res. and Rev.*, **1**, 75-88.

4. Mrvaljevic, Rosalinda K., Peter G. Black, Luca R. Centurioni, Eric A. D'Asaro, Craig Lee, Ren-Chieh Lien, Jan Morzel, Pearn P. Niiler, Luc Rainville, Thomas B. Sanford, and T. Y. Tang, 2013: Observations of the cold wake of Typhoon Fanapi, *Geophys. Res. Letters*, **40**, *2*, 316-321

5. Katsaros, K., L. Mitnik and P. Black, 2012: Innovative microwave instruments for observing tropical cyclones, Chapt 2, **Typhoon Impacts and Crisis Management**, Danling Tang, ed., Springer

6. Lin, I-I, P. Black, J. F. Price, C-Y Yang, S/. S. Chen, C-C Lien, P. Harr, N-H Chi, C-C Wu and E. A. D'Asaro, 2013: An ocean cooling potential intensity index for tropical cyclones, *Geophys. Res. Letters*, *Geophys. Res. Letters*, **40**, 1878-1882.

7. D'Asaro, E.A., P.G. Black, L.R. Centurioni, Y.-T. Chang, S.S. Chen, H.C. Graber, P. Harr, Verena Hormann, R.-C. Lien, I.-I. Lin, T.B. Sanford, T.Y. Tang, and C.-C. Wu, 2013: Impact of typhoons on the ocean in the Pacific: ITOP, *Bull. Amer. Meteorol. Soc*., accepted.

Selected conference presentations or papers.

1. **AGU 2012 Fall Meeting:** Observation of C-band brightness temperature from the Hurricane Imaging RADiometer (HIRAD) on-board the NASA WB-57 during GRIP in Hurricanes Earl and Karl (2010): Timothy Miller, Mark James, J. Brent Roberts, Sayak Biswas, Eric Uhlhorn, Robert Atlas, Peter Black, W. Linwood Jones, Jimmy Johnson, Spencer Farrar, Saleem Sahawneh, Christopher Ruf and Marry Morris

2. **AGU 2012 Fall Meeting:** Validation of Air-Ocean-Wave Coupled Simulation of Typhoon Fanapi: S. Chen; P. Harr; R. Elsberry; M. Peng; P.G. Black; J.M. Schmidt; R. Mrvaljevic; E.A. D'Asaro; T.B. Sanford; L.R. Centurioni; J. Morzel; H.C. Graber

3. **AGU 2012 Fall Meeting:** Formation and Recovery of Cold Wake during Typhoon Fanapi (2010): S. Wang; H. Jin; P.G. Black; S. Chen; J. Doyle; L.W. O'Neill

4. **AGU 2012 Fall Meeting:** An Ocean-Based Potential Intensity Index for Tropical Cyclones: I.I. Lin; P.G. Black; J.F. Price; C. Yang; S.S. Chen; N. Chi; P. Harr; C. Lien; E.A. D'Asaro; C. Wu

5. ***AMS Annual Meeting, 17th Conference on Integrated Observing and Assimilation Systems for Atmosphere, Oceans, and Land Surface (IOAS-AOLS):*** Use of airborne and satellite observations to diagnose typhoon-ocean interactions and extreme-wind boundary layer structure during ITOP2010: Peter G. Black, SAIC/NRL, Monterey, CA; and R. Mrvaljevic and A. B. Penny

6. **AMS Annual Meeting, 17th Conference on Integrated Observing and Assimilation Systems for Atmosphere, Oceans, and Land Surface (IOAS-AOLS):** Observations of C-band brightness temperatures and ocean surface wind speed and rain rate from the Hurricane Imaging Radiometer (HIRAD) during GRIP and HS3: Timothy L. Miller, NASA/MSFC, Huntsville, AL; and M. W. James, J. B. Roberts, W. L. Jones, S. Biswas, C. S. Ruf, E. Uhlhorn, R. Atlas, P. G. Black, and C. M. Albers

7. **67th Interdepartmental Hurricane Conference:** Outflow Layer Structure in Hurricanes Leslie And Nadine Revealed by Dropsondes Deployed from NASA Global Hawk UAV Aircraft during the 2012 Hurricane and Severe Storms Sentinel (HS3) Campaign: A New TC Observational Strategy: *Peter G. Black* (SAIC/NRL Monterey), Jon Moskaitis, James Doyle, Chris Velden, and Scott Braun

8. **67th Interdepartmental Hurricane Conference:** Implementation of Upper-Ocean Temperature Measurements on Operational Hurricane Reconnaissance: An Update on the AXBT Demonstration Project: *Elizabeth R. Sanabia* and Bradford S. Barrett (USNA), Peter Black (SAIC/NRL Monterey), Sue Chen and James Cummings (NRL Monterey)